ISSN 1330–0008
CODEN FIZAE4

STRUCTURE OF BALL MILLED ZrO_2 AND ZrO_2 -10 mol % Y_2O_3 POWDERS REVEALED BY HRTEM IMAGE PROCESSING

ANĐELKA M. TONEJC, IGOR DJERDJ and ANTUN TONEJC

Department of Physics, Faculty of Science, Bijenička 32, POB 331, 10002 Zagreb, Croatia
E-mail: andelka@phy.hr

Dedicated to Professor Kseno Ilakovac on the occasion of his 70$^{\mathrm{th}}$ birthday

Received 18 October 2001; Accepted 7 January 2002
Online 6 April 2002

High-resolution transmission electron microscope (HRTEM) image processing analysis is used to analyse and to compare the process of ball milling in pure ZrO_2 powders and in ZrO_2-10 mol % Y_2O_3 powders. Applying HRTEM image processing to the grain boundary region and other defects, we are able to observe, at the atomic level, a possible sequence of alloying and transition that occur at the grain boundary, in the overlapping layers and on the stacking faults.

PACS numbers: 61.43.Gt, 68.37.Lp UDC 537.533.35

Keywords: ZrO_2 powder, ZrO_2-10 mol % Y2O$_3$ powder, ball milling, high-resolution transmission electron microscopy, image processing, grain boundaries, overlapping layers, stacking faults

1. *Introduction*

In the last 15 years, zirconia (ZrO_2) and its solid solutions (stabilised zirconia ceramics) have attracted great attention from scientists and technologists in different fields due to their mechanical, thermal, electrical and optical properties.

At atmospheric pressure, ZrO_2 has three polymorphs: monoclinic (m), tetragonal (t) and cubic (c) phase. The temperatures of phase transitions are: m $\rightarrow$ t at 1150 °C; t $\rightarrow$ c at 2370 °C; and c $\rightarrow$ up to the melting point at 2680 °C. At high pressure, the orthorhombic phase has been observed. Monoclinic ZrO_2 has the space group $P2_1/c$; its unit cell contains four formula units ZrO_2; the unit cell parameters are $a = 0.53129$ nm, $b = 0.52125$ nm, $c = 0.51471$ nm, $\beta = 99.218°$. Coordination number of Zr atom is 7; Zr–O distances are 0.205 nm and 0.228 nm.

Zirconia and its solid solutions were elaborated in many articles [1–3]. The transitions in zirconia are martensitic, having the determined crystallographic relationship for the single crystals: $(001)_t \parallel (001)_m$ [1]. The transitions in pure zirconia are associated with large volume changes, which makes the material useless at high temperature due to cracking. However, stabilisation of the high temperature cubic phase to the room temperature is possible by alloying zirconia with other oxides, such as MnO, NiO, Cr_2O_3, Fe_2O_3, Y_2O_3 and Ce_2O_3. But a very high temperature (over 1000 °C) of calcination or sintering is required for preparation of solid solutions of zirconia with these oxides [4–6]. This rather high temperature procedure can be avoided by using the mechanical alloying (MA) in high-energy mechanical ball mills. The mechanical alloying (MA) has been extensively used in the last 20 years as a non-equilibrium processing method, for synthesizing, at room temperature, all kinds of materials (intermetallic compounds, solid solutions and even those which are immiscible by conventional processing methods) [7]. Furthermore, the decrease of the grain size to nano-size dimensions has become a common feature of the mechanical milling process [7].

In 1993, Y. L. Chen and D. Z. Yang showed [8] that by using the mechanical alloying, they were able to synthesize the ZrO_2-CeO_2 solid solution, and in 1996, A. M. Tonejc and A. Tonejc reported [9] about the MA of other zirconia solid solutions, ZrO_2 − 10 mol % of Y_2O_3 (CoO, Fe_2O_3, or α-Al_2O_3). Although in the first stages of the alloying, the tetragonal phase appeared, the end product was a cubic solid solution [10].

The milling experiments performed by J. E. Bailey et al. [11] also showed that it is possible to transform monoclinic zirconia to tetragonal. They suggested that the transition appeared due to the reduction of the crystallite size down to 5 nm. However, the transition was not complete. The amount of the tetragonal phase was limited to approximately 45%, even after a prolonged milling.

The mechanical alloying and grinding of materials have been shown complex and it is not a surprise that the models describing the processes are still under debate [12–14]. The model which is mostly accepted includes a kind of solid-state reaction between thin layers which appear during successive fracturing and welding of particles that are steadily trapped between colliding balls or between the ball and vial [15,16]. Only a few papers have been published on the use of TEM and HRTEM investigation to confirm the model of alloying process [17–21], and only two papers in which HRTEM image processing analysis was applied to explain the mechanical alloying process [17,19].

In this paper we will intend to give a further insight into the initial stages of MA in ZrO_2-10 mol % Y_2O_3 powders as well as into the monoclinic-tetragonal phase transition in ball milled (BM) pure ZrO_2 powders obtained by different preparation procedures.

2. *Experimental procedure, TEM, HRTEM and image processing*

Powders of zirconia and yttria were milled in a Fritsch planetary micro-ball mill Pulverisette 7, having a tungsten carbide vial and balls, as reported previously [9]. The resulting samples were examined by X-ray diffraction, by TEM, HRTEM, selected area electron diffraction (SAED) and energy dispersive spectroscopy (EDS). The JEOL JEM 2010 electron microscope was used (the acceleration voltage of 200 kV; C_s 0.5 mm; the point resolution of 0.19 nm).

X-ray diffraction measurements were performed at room temperature using a Philips (PW 1820) powder diffractometer, with monochromatized CuKα radiation. The lines of an iron sample holder were used as a reference. Philips PC-APD version 3.5 b software based on Marquand non-linear least-squares algorithm was used for line-profile analysis and peak-position measurements. The fraction of tetragonal phase (t) was estimated from the ratio of peak intensities according to the equation [11]

$$t = \frac{I_t(111)}{I_t(111) + I_m(--111) + I_m(111)} \,. \tag{1}$$

The TEM analysis of starting powders used in milling experiment showed the phase composition (m-monoclinic, t-tetragonal) and average grain size as follows:

- First ball milled experiment: m+t-ZrO_2 (J.S. white); average grain size $D =$ 14.7 nm (from dark field TEM)
- Second ball milled experiment: m-ZrO_2 (Ventron white); average grain size $D = 460$ nm (from dark field TEM)
- Third ball milled experiment: m-ZrO_2 (Ventron)+Y_2O_3; the results are given in Refs. [9], [17] and [19].

HRTEM images were digitised by a scanner and analysed with the CRISP programme [22]. The basic principle is: The transition from the direct to the reciprocal space in the back focal plane of the objective lens through the gate of Fourier transforms (FT). The Fourier transforms of regions of size 256×256 pixels (corresponding to around 8 nm x 8 nm in the specimen) were calculated. In each FT, masks with holes of radius 5 pixels were used to select components of the FT. The effect of the holes size was investigated within a range from 1 to 5 pixels, the largest size being chosen in order to ensure that very strong reflections from ZrO_2 were completely encircled by the mask hole.

3. *XRD results*

For the purpose of this research, we took the XRD patterns of the starting powder samples and of milled samples of ZrO_2. The series of XRD patterns of ball-milled m-ZrO_2 samples for different milling times are shown in Fig. 1. The XRD patterns of the starting m-ZrO_2 Ventron powder is shown in Fig. 2d.

Using Eq. (1), the starting composition of (m+t) ZrO_2 was 69% m-ZrO_2 and 31% t-ZrO_2. It transformed to 50% t-ZrO_2 after 80 minutes of milling.

After 180 minutes of ball milling of m-ZrO_2 Ventron powder, the estimated fraction of the tetragonal phase was approximately 26%.

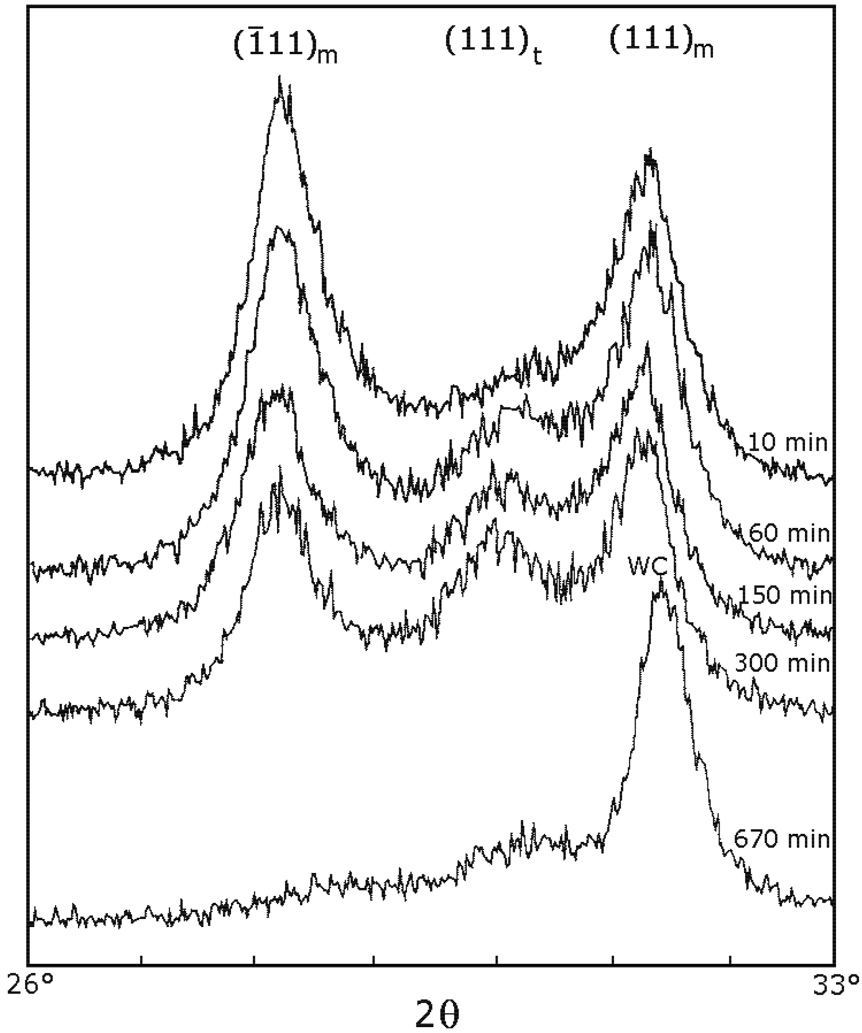

Fig. 1. XRD patterns of ZrO_2 *powder milled for different milling times (10, 60, 150, 300 and 670 minutes), recorded in the range of 2θ from 26° to 33°. The strongest monoclinic (–111) and (111), and tetragonal (111) reflections are marked.*

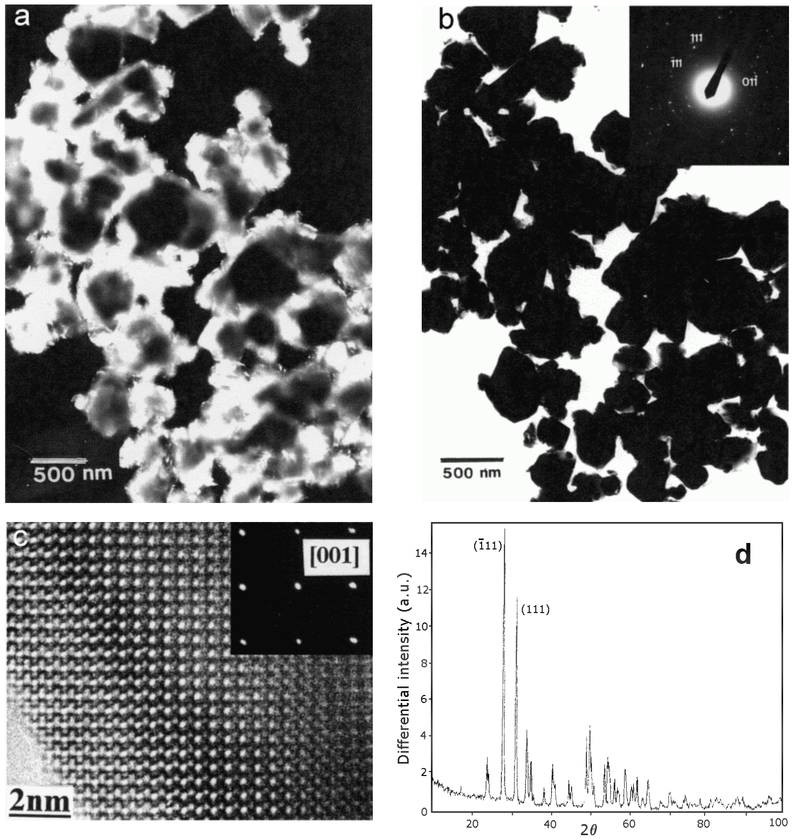

Fig. 2. (a) Dark field (DF) image of as-prepared ZrO_2 *(Ventron white) taken with (111)-spot of monoclinic* ZrO_2 *from corresponding SAED pattern given in the inset of Fig. 2b; (b) Bright field (BF) image of* ZrO_2 *(Ventron white); (c) HRTEM image of* ZrO_2 *(Ventron white) viewed along the [001] direction. Corresponding SAED pattern is shown in the inset; (d) XRD pattern of as-prepared* ZrO_2 *(Ventron white).*

4. TEM and HRTEM results; image processing analysis

4.1. HRTEM image processing of ZrO_2 photographs

In Fig. 2a, there is a dark-field image of ZrO_2 powder used in BM procedure (Ventron white) taken with the (111) spot of m-ZrO_2 from the corresponding SAED pattern given in the inset of the bright field image (Fig. 2b). The average grain size of the non-milled zirconia measured from Fig. 2a was 460 nm, and from SAED pattern it appears completely monoclinic, which is in accordance with the XRD results (Fig 2d). Figure 2c shows HRTEM image of one monoclinic grain oriented in the [001] direction of the corresponding SAED pattern (inset).

Figure 3 is a HRTEM image of the ZrO_2-Ventron powder milled for 150 minutes. Since the sample was completely monoclinic before milling, we have been interested in the appearance of tetragonal ZrO_2. The areas used for analysis, marked 1 and 2, contain grain boundaries GB1 and GB2, formed of two grains (A and B) and at least three grains, respectively. The calculated Fourier transform (FT) corresponds to the diffraction pattern of the image. Each distinctive set of planes in the image will give a Fourier component in the calculated diffraction pattern, a bright spot (a "reflection") with a given amplitude and phase. Filtering of the spots in the diffraction pattern allows individual features in the original image to be reconstructed. Using the CRISP approach [22] to image processing, we can obtain information about the particular family of crystal planes and about the structure of crystal lattice.

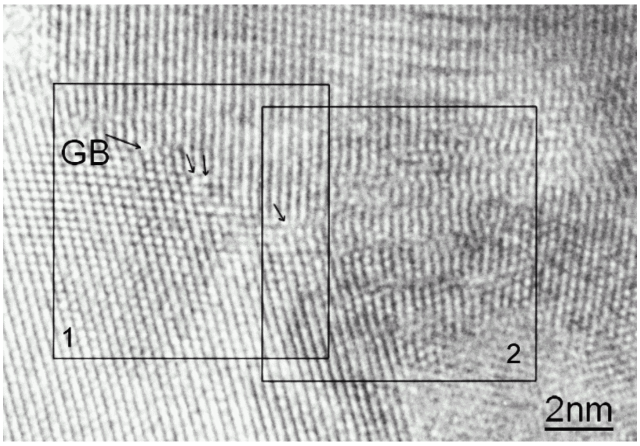

Fig. 3. HRTEM image of m-ZrO_2 *(Ventron white), BM for 150 minutes. The areas 1 and 2 used for image processing are marked with black squares. Black arrows indicate dislocations positioned at grain boundary (GB).*

4.1.1. **Grain boundary 1 (GB1)**

The analysis of GB1 is displayed in Figs. 4a to 4m and in Table 1. The original image is given in Fig. 4l, and its FT in Fig. 4m. GB1 is the region between grains A

Fig. 4 (at right). Filtered lattice images of GB1 from HRTEM image of ZrO_2 *(150 minutes milled Ventron white), area 1 from Fig. 3, obtained with particular diffraction spots from FT of Fig. 4m: (a) spot* 1^A*-(–111)* m-ZrO_2, $d = 0.316$ nm*; (b)* 1^B*-(111)* t-ZrO_2, $d = 0.296$ nm*; (c) 2-(002)/(200)-*ZrO_2 *(t/m),* $d = 0.260/0.262$ *nm; (d) 3-(011) m-*ZrO_2*,* $d = 0.363$ *nm; (e) 4-(113)* t-ZrO_2*,* $d = 0.157$ *nm; (f) 5-(–111)* m-ZrO_2, $d = 0.316$ nm*; (g) 6-(–111)* m-ZrO_2, $d = 0.316$ nm*; (h) 7-(111)* t-ZrO_2, $d = 0.296$ nm*; (i) reconstructed original image with all reflections assigned to tetragonal (t)* ZrO_2*; (j) reconstructed original image with all reflections assigned to monoclinic (m)* ZrO_2*; (k) reconstructed original image with all reflections from FT; (l) original image; (m) FT of the region.*

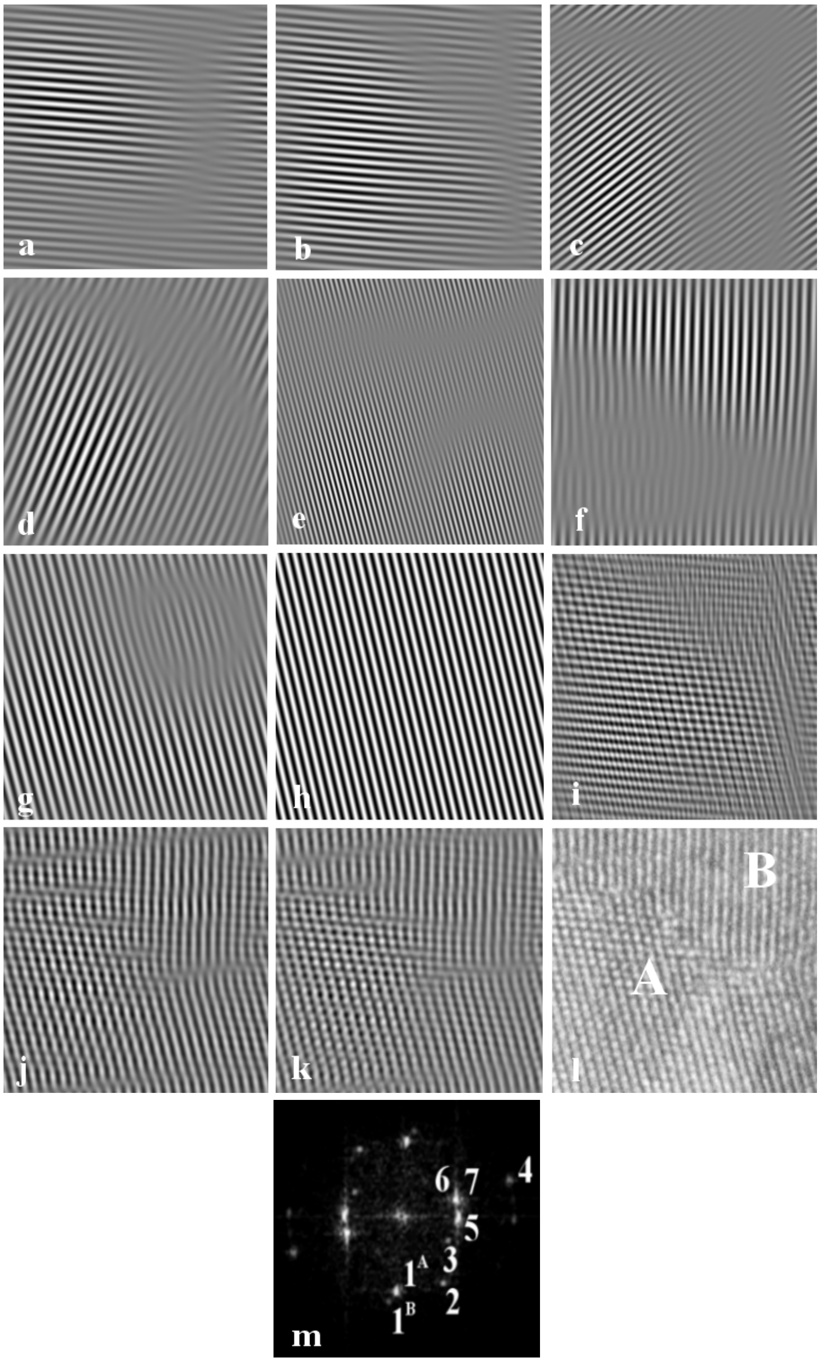
a
b
c
d
e
f
g
h
i
j
k
l
B
A
m
6 7
4
5
1A
3
2
1B

TABLE 1. Grain boundary (GB1) of ball-milled ZrO_2 *for 150 minutes; d-value assignments belonging to FT (Fig. 4m); m-monoclinic, t-tetragonal.*

Spot in FT	d (nm) (measured)	h, k, l (calc.)	Phase identified	d(nm) (from lit.)	Corresponding lattice image
1A	0.3000–0.3215	–111	m	0.3164	Fig. 4a
1B	0.2898–0.3000	111	t	0.2960	Fig. 4b
2	0.2638–0.2702	002/200	t/m	0.2600/0.2622	Fig. 4c
3	0.3597–0.3663	011	m	0.3639	Fig. 4d
4	0.1592–0.1647	113	t	0.1575	Fig. 4e
5	0.3115–0.3344	–111	m	0.3164	Fig. 4f
6	0.3125–0.3355	–111	m	0.3164	Fig. 4g
7	0.2932	111	t	0.2960	Fig. 4h

and B. The image size is 256×256 pixels, corresponding to 8 nm × 8 nm. Numbers 1 to 7 mark reflections in FT and their identification is given in Table 1. The reflection marked 1 was a complex elongated spot containing two components, 1A and 1B. The evidence about a layered structure formed during milling could be obtained if we assign 1A and 1B to (–111) m-ZrO_2 and (111) t-ZrO_2, respectively. The inverse FT, i.e. filtered lattice images of the m-ZrO_2 (–111) reflection and of the (111) t-ZrO_2 reflection, are given in Figs. 4a and 4b, respectively.

This could mean that one part on this particular grain belongs to t-ZrO_2 and the other to m-ZrO_2. The reflection marked 2 could be assigned to m-ZrO_2 (200) and t-ZrO_2 (002) as well. Its inverse FT is given in Fig. 4c, revealing lattice image in real space. According to this assignment, we can determine the orientation relationship between parent monoclinic and nucleated tetragonal phase, $(200)_m \parallel (002)_t$. This result confirms the lattice correspondence between monoclinic and tetragonal phases, established by Stubičan [1], which fulfils the necessary condition for the existence of a coherent boundary between the two phases. Figure 4d shows the (011) lattice image of m-ZrO_2 obtained using reflection 3. Figure 4e shows the (113) lattice image of t-ZrO_2 obtained using reflection 4, corresponding to grain A. Similarly, Fig. 4f shows the lattice image of the (–111)-m from reflection 5 which corresponds to grain B, and Fig. 4g shows the (–111)-m lattice image obtained using spot 6. Reflection 7 with the corresponding lattice image given in Fig. 4h belongs to t-ZrO_2. This is another evidence of the presence of tetragonal zirconia in the monoclinic ZrO_2 grain. The reconstruction, using all tetragonal reflections from FT, is given in Fig. 4i, while reconstruction using all monoclinic reflections is given in Fig 4j. The original reconstructed image is given in Fig. 4k. The superposition of tetragonal and monoclinic layers in the grain A is obvious.

4.1.2. **Grain boundary 2 (GB2)**

The results of filtering analysis of region 2 (Fig. 5e) from Fig. 3 are displayed in Figs. 5a to 5f. In FT of Fig. 5f, three strong spots are marked. They are assigned to (–111)m- ZrO_2, and the corresponding planes are shown on Figs. 5a, 5b and 5c. The original reconstructed image (Fig. 5d) shows interesting features, which confirms our assumption about the influence of ball milling to morphology (disorder level, strain) of the nanocrystalline sample. This image shows a rupture of (–111) m-ZrO_2 planes, and insertion of other (–111) planes of ZrO_2. The rupture of planes in the ball-milled sample occurs at the level of 1.3 nm, shown by arrows in Fig. 5d. By comparison of the lattice images from Figs. 5a, 5b, 5c, and reconstructed original image 5d, we can observe how different planes of m-ZrO_2 lattice images are settled in the GB2 region. In the reconstructed image, the dislocation array is revealed, with average distance between dislocations of 1.3 nm.

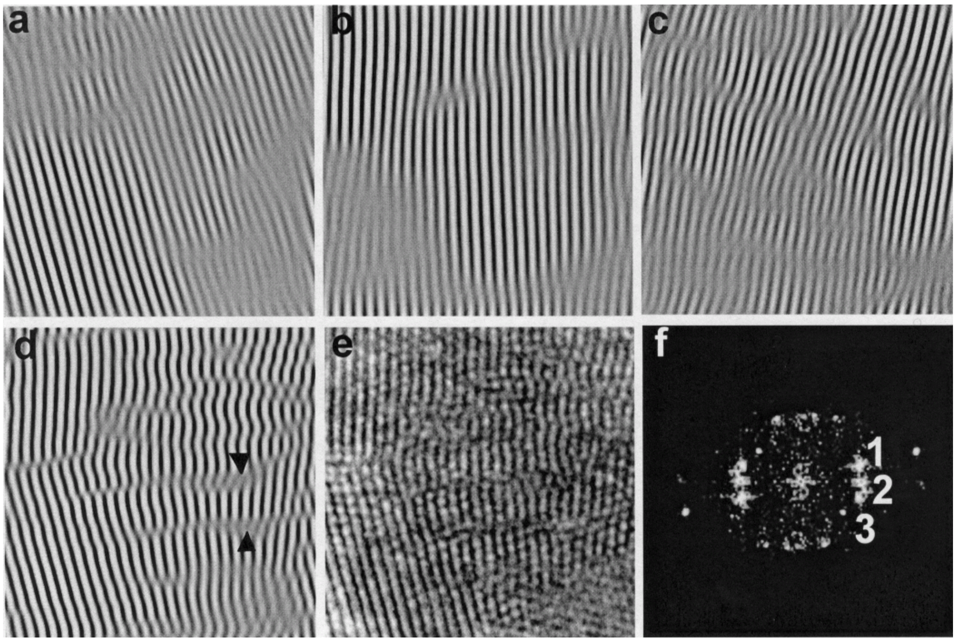

Fig. 5. Filtered lattice images of GB2 from HRTEM image of the sample ZrO_2 *(150 minutes milled Ventron white) area 2 from Fig. 3, obtained with particular diffraction spots from FT of Fig. 5f: (a) spot 1-(–111)* m-ZrO_2, d = 0.316 nm*; (b) 2-(–111)* m-ZrO_2, d = 0.316 nm*; (c) 3-(–111)* m-ZrO_2, d = 0.316 nm*; (d) reconstructed original image with all reflections from FT; (e) original image; (f) FT of the region.*

4.1.3. **Uniaxial ordering in BM (m+t) ZrO_2 powders**

Using image-processing analysis, we observed interesting phenomena which appeared during the milling process. One of the events is revealed in Figs. 6a – 6f. In Fig. 6f, there is an 11 nm × 11 nm region of HRTEM image of ZrO_2 sample milled for 15 min (J. S. white). Its FT is given in Fig. 6g, and spots numbered 1 to

3 are marked. Their assignment is given in Table 2. We observe that spots 1 and 2 show different intensities, the spots are along straight lines, ratio of their *d*-values is 2, which indicates the appearance of nanoscale ordering in m-ZrO_2 lattice. This ordering, observed in many different HRTEM images of ball milled ZrO_2, is a phenomenon which appears and disappears during the BM process and consequently represents a metastable state. The lattice fringes obtained using spot 1 are given in Fig. 6a, and are assigned to (001)m-ZrO_2. Similarly, using spots 2 and 3, the lattice

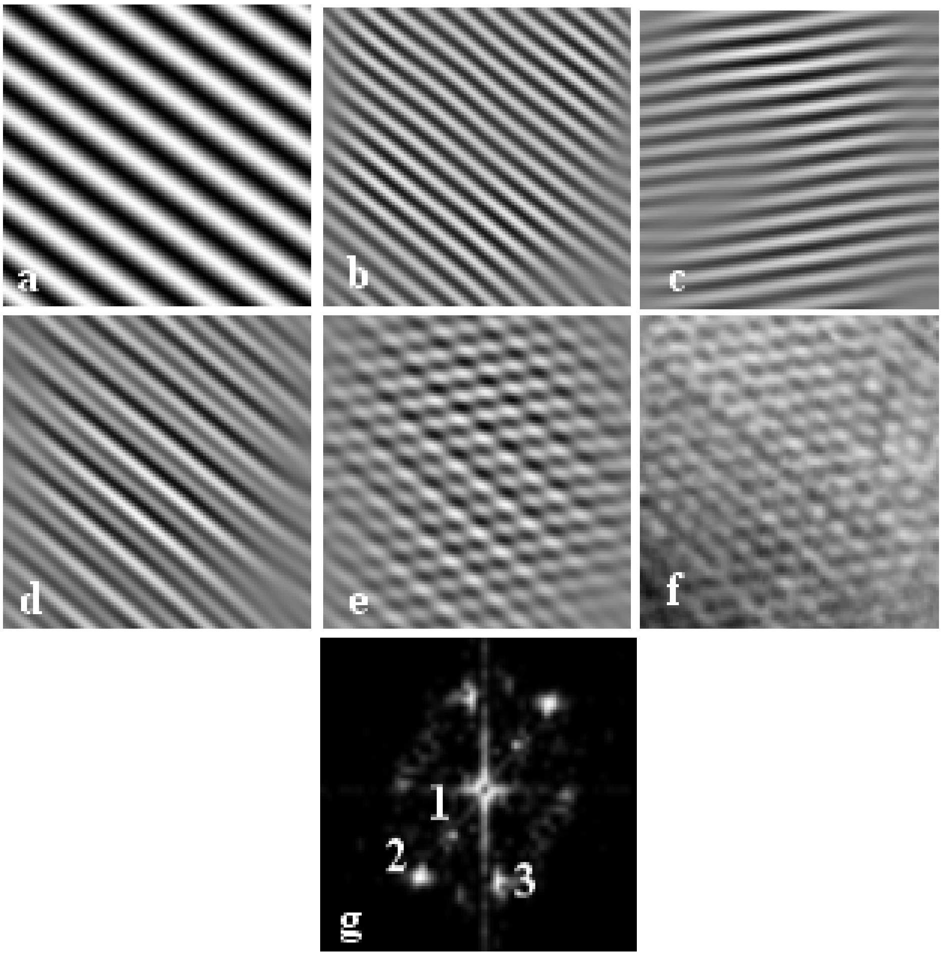

Fig. 6. Filtered lattice images of HRTEM image of sample ZrO_2 *(15 minutes milled J. Stefan) obtained with particular diffraction spots from FT of Fig. 6g: (a) spot 1 -(001)* m-ZrO_2, $d = 0.508$ nm*; (b) 2-(002)* m-ZrO_2, $d = 0.253$ nm*; (c) 3-(–111)* m-ZrO_2, $d = 0.316$ nm*; (d) superposition of filtered images a) and b); (e) reconstructed original image with all reflections from FT; (f) original image; (g) FT, reflections 1, 2, 3, give filtered images in (a), (b), (c).*

TABLE 2. Uni-axial ordering in ball-milled ZrO_2 *for 15 minutes (J. Stefan white); d-value assignments belonging to FT (Fig. 6g); m-monoclinic.*

Spot in FT	d (nm) (measured)	h, k, l (calc.)	Phase identified	d(nm) (from lit.)	Corresponding lattice image
1	0.5235	001	m	0.5087	Fig. 6a
2	0.2538–0.2890	002	m	0.2539	Fig. 6b
3	0.3118–0.3436	–111	m	0.3164	Fig. 6c

images shown in Figs. 6b and 6c are obtained, respectively. They are assigned to (002)m- and (−111)m-ZrO_2. The superposition of lattice images, shown in Figs. 6a and 6b, is given in Fig. 6d. It clearly shows two different sets of crystallographic planes. The original reconstructed image is given in Fig. 6f.

4.2. *HRTEM image processing of ZrO_2-Y_2O_3 photographs*

X-ray diffraction (XRD) in ZrO_2-10 mol % Y_2O_3 powders ball milled for 10 minutes showed evidence of the formation of tetragonal zirconia solid solution (t-ZrO_2 SS) [9].

From the previous TEM, HRTEM and electron diffraction (ED) measurements [17], we obtained evidence of the microstructure in different regions of the sample. We observed the agglomeration of t-ZrO_2 and Y_2O_3 grains (from 7 to 60 nm) attached to a large m-ZrO_2 grain. The layered structure, induced by ball milling, revealed the shear deformation of lattice planes and planes ruptures. The small flakes of material having sizes of 10 nm possessed, according to SAED [17], a tetragonal nanocrystalline structure. These first grains of t-ZrO_2 solid solution were nucleated at m-ZrO_2 grains.

Further insight into the alloying process could be obtained by image processing of HRTEM photographs. We analysed [17,19,23] the grain boundary regions, GB, overlapping layers of zirconia and yttria and the region containing stacking faults.

From those analyses using Fourier filtering (and reconstruction of original image), we revealed at the atomic level one possible sequence of alloying that occurred at the grain boundary, on stacking faults and in the overlapping layers.

5. *Discussion*

According to the temperature diagram of ZrO_2, monoclinic to tetragonal phase transition takes place at 1150 °C [1]. Generally, the experiments with ball milling show the possibility of existence of the high-temperature phase at the room temperature [18]. Summarising our image processing analysis, we can reveal a large amount of defects, dislocations, grain boundaries (GB), overlapped grains and layers. Moreover, as seen in Fig. 3, dislocations (denoted by black arrows) are stacked at obstacles such as denoted GB1 analysed in Fig. 4. At shorter milling times, we observed the type of GB1 more frequently, while for longer milling times, the nanocrystalline GB2 is observed in milled ZrO_2 as well as in ZrO_2 -Y_2O_3 powders.

Due to the nanocrystalline nature of our samples, there is a large fraction of grain boundaries. Their volume fraction can be expressed [24] as

$$f_{\mathrm{GB}} = 1 - \left(\frac{D}{D+d} \right)^3 , \tag{2}$$

where D is the grain diameter and d the thickness of GB (usually taken as 1 nm). If we apply Eq. (2) for the average grain size, we obtain for a sample milled for 150 minutes $f_{\mathrm{GB}} = 23.5\%$. In the calculation of the average grain size for milled zirconia, we used an average grain size of monoclinic and tetragonal phase volume weighted. This means that with decreasing of the average grain size, GB will take a large fraction of the whole volume. Such a large amount of interfaces will obviously increase the free energy of a system. Let us denote by G_{tm} and G_{tt} the total free energy of monoclinic and tetragonal phase, respectively, and ΔG the free energy increase of monoclinic phase due to defects (strain energy). When the equation

$$G_{\mathrm{tm}} + \Delta G > G_{\mathrm{tt}} \tag{3}$$

is satisfied, tetragonal phase can be formed, even at the room temperature. Since the surface-to-volume energy ratio is relatively large for nanocrystalline materials, the basic contribution to the free energy is the surface energy contribution. Qi et al. [24] showed in a simple thermodynamic approach that the increase of free energy ΔG due to defects induced by ball milling is proportional to the volume fraction of interfaces, f_{GB}, which relates to the grain size through Eq. (2). On the basis of this approach, they estimated the critical grain size diameter below which tetragonal phase is stable ($D_{\mathrm{c}} = 12.3$ nm). Our result (XRD) for average grain size of the tetragonal form (7 nm) is in accordance with Qi's result [24]. This model of increase of free energy due to the increase of defect concentration can explain not only the monoclinic to tetragonal phase transition, but also the reverse process, the tetragonal ZrO_2 phase transforms to m-ZrO_2 at the ambient temperature.

The order-disorder process, revealed by HRTEM image processing and observed locally in BM ZrO_2 powders, could help in explaining the transition from m- to t-ZrO_2, as was reported earlier in other ball-milled systems [25].

6. Conclusion

From the TEM, HRTEM and image processing analyses of ball-milled ZrO_2 powders, we obtained the following results:

a) A decrease of the grain sizes with milling time.

b) The appearance of defects: dislocations at the grain boundary (GB) and dislocations forming nanocrystalline GB, some stacking faults (SF).

c) In some regions of the samples, the uni-axial ordering was observed.

d) We did not observe a complete transition to t-ZrO_2 in our experiments. In m-ZrO_2-Y_2O_3 milling experiments, a complete transition to t-ZrO_2 and after that to cubic c-ZrO_2 solid solution was obtained.

Using the HRTEM image processing analysis of ZrO_2-Y_2O_3 powders [17,19], it was possible to conclude the following:

a) The formation of the layered structure and growth of t-ZrO_2 in monoclinic matrix.

b) The formation of defects: dislocations (ZrO_2 planes or Y_2O_3 planes) in GB region; stacking faults which accommodate the interface between grains; plane rupture; enhancement strain level (strain free energy) and probability from m- to t-ZrO_2 transition.

c) The decrease of grain sizes is accompanied by stresses in BM process when the defects are formed; Fourier filtering analysis assigns inserted planes to particular planes having origin in ZrO_2 or Y_2O_3 planes, according to the corresponding FT of the region.

d) As observed by HRTEM [17,19], the alloying could be considered as interpenetration of ZrO_2 and Y_2O_3 planes into the GB; the other mechanism of alloying proceeds via the segregation of Y_2O_3 on the stacking faults in m-ZrO_2.

Acknowledgements

We gratefully acknowledge the financial support from the Ministry Science and Technology of Croatia.

References

[1] V. S. Stubičan, *Crystallography and Applications of Zirconia and Zirconia Solid Solutions*, *Proc. Yugoslav Centre of Crystallography* **20** (1985) 5.

[2] E. C. Subbaro, H. S. Maiti and K. K. Srivastava, phys. stat. sol. (a) **21** (1974) 9.

[3] J. Z. Jiang, F. W. Poulsen and S. Mörup, J. Mater. Res. **14** (1999) 1343.

[4] G. K. Bansal and A. H. Heuer, Acta Metall. **20** (1972) 1281.

[5] A. Keshavaraja and A. V. Ramaswamy, J. Mater. Res. **9** (1994) 837.

[6] M. C. Caracoche, P. C. Rivas, A. P. Pasquevich and A. R. Lopez Garcia, J. Mater. Res. **8** (1993) 605.

[7] A. W. Weeber and H. Bakker, Physica B **153** (1988) 93.

[8] Y. L. Chen and D. Z. Yang, Scr. Met. **29** (1993) 1349.

[9] A. M. Tonejc and A. Tonejc, Mat. Sci. Forum **225–227** (1996) 497.

[10] A. Sekulić, K. Furić, A. Tonejc, A. M. Tonejc and M. Stubičar, J. Mater. Sci. Letters **16** (1997) 260.

[11] J. E. Bailey, P. M. Bills, Z. M. Librant and D. Lewis, Trans. J. Brit. Cer. Soc. **71** (1972) 25.

[12] E. Gaffet and F. Bernard, J. Mater. Chem. **9** (1999) 305.

[13] P. J. Desré and A. R. Yavary, Phys. Rev. Lett. **64** (1990) 1533.

[14] A. R. Yavary and P. J. Desré, Mater. Sci. Eng. A **134** (1991) 1315.

[15] M. Seidel, J. Eckert, I. Bächer, M. Reibold and L. Schulz, Acta Mater. **48** (2000) 3657.

[16] R. B. Schwartz, Mater. Sci. Forum **269–272** (1998) 665.

[17] A. M. Tonejc, A. Tonejc, G. W. Farrants and S. Hovmöller, Croatica Chem. Acta **72** (1999) 311.

[18] T. Chen, J. M. Hampikian and N. N. Thadhani, Acta Mater. **47** (1999) 2567.

[19] A. M. Tonejc, Acta Chim. Slov. **46** (1999) 435.

[20] A. M. Tonejc, D. Bagović and M. Tudja, Mater. Lett. **20** (1994) 51.

[21] J. Eckert, L. Schultz and K. Urban, J. Non-Cryst. Solids **130** (1991) 273.

[22] S. Hovmöller, Ultramicroscopy **41** (1992) 121.

[23] A. M. Tonejc, A. Tonejc, G. W. Farrants and S. Hovmöller, Mat. Sci. Forum **357–362** (1998) 269.

[24] M. Qi and H. J. Fecht, Mat. Sci. Forum **269–272** (1998) 187.

[25] M. S. Kim and C.C. Koch, J. Appl. Phys. **61** (1987) 3450.

OTKRIVANJE STRUKTURE KUGLAMA MLJEVENIH PRAHOVA ZrO_2 I ZrO_2 -10 mol % Y_2O_3 OBRADOM SLIKA HRTEM

Primijenili smo analizu obradom slika iz transmisijskog elektronskog mikroskopa visokog razlučivanja (HRTEM) radi usporedbe procesa mljevenja kuglama čistog praha ZrO_2 i praha ZrO_2-10 mol % Y_2O_3. Primjenom obrade slika HRTEM za granične dijelove zrnaca i za druge defekte, uspjeli smo, na atomskoj razini, opažati moguće sljedove tvorbe slitina i prijelaza koji se dešavaju na granicama zrnaca, u preklopima slojeva i u pogreškama gomilanja.